Les Cahiers du GERAD ISSN: 0711–2440

Risk-resilient mine production schedules yielding favourable product blends for rare earth element deposits

M. Quigley,
R. Dimitrakopoulos

G–2016–102

November 2016

GERAD HEC Montréal
3000, chemin de la Côte-Sainte-Catherine
Montréal (Québec) Canada H3T 2A7

Tél. : 514 340-6053
Téléc. : 514 340-5665
info@gerad.ca
www.gerad.ca

Risk-resilient mine production schedules yielding favourable product blends for rare earth element deposits

Matthew Quigley [a]

Roussos Dimitrakopoulos [a, b]

[a] *COSMO Stochastic Mine Planning Laboratory, Department of Mining and Materials Engineering, McGill University, Montréal (Québec) Canada, H3A 0E8*

[b] *GERAD Montréal (Québec) Canada, H3T 2A7*

matthew.quigley@mail.mcgill.ca
roussos.dimitrakopoulos@mcgill.ca

November 2016

Les Cahiers du GERAD

G–2016–102

Abstract: Recent developments in the global rare earth elements (REE) sector have caused a surge in motivation for nations outside of China to secure their own REE supply. However, the volatility of this sector is hindering most of these projects from reaching production. The aim of this study is to address one of these major sources of risk: the inherent geological uncertainty of REE deposits. By deterministically estimating ore quality and assuming the distribution of REEs present in a deposit using the total rare earth oxide (TREO) grade, a mine planner does not have the necessary resolution to properly assess these risks and inform their decisions. As a result, the mine production schedule will not maximize the generation of cash flows nor meet the expected production targets. Better representation of a REE deposits' spatial variability and uncertain characteristics, coupled with advancements in the field of stochastic mine planning, can offer the tools to develop a mine design that will yield a higher NPV while ensuring a better performance in terms of achieving ore tonnage, ore grade and desired blend of REE mineralization goals. The application herein will consist of the joint conditional simulation of the 14 stable Lanthanides and Yttrium present in a monazitic REE deposit. Multiple realizations of this deposit are used to develop a risk resilient mine production schedule that will maximize NPV while ensuring consistent ore grades and REE blends at the head of the mill.

1 Introduction

The term “Rare Earth Elements” (REE) is used to describe 17 chemically similar elements of the periodic table, including scandium, yttrium and the 15 elements of the lanthanide series. Their unique chemical and physical properties are critical in driving strategic industries such as renewable energy, communications, defence, healthcare, advanced optics and many other high tech sectors that have gained popularity in the 21st century. For the last decade, China has dominated the global production and consumption of REE products accounting for approximately 83% and 70%, respectively (Roskill, 2014). China’s tremendous demand for REE is only expected to increase over the course of the next decade as they move towards high tech industry and clean energy initiatives. In 2011, China drastically tightened their REE export quotas, causing prices to skyrocket as the risk of an impending global supply shortage became apparent. This monopoly, paired with the expected increase in REE demand, brought global attention to the imminent supply risk of these metals. To secure and maintain competitive rare earth market share, nations such as Australia, Japan, South Korea, the USA and Canada have initiated government and industry funded programs to secure resource supply, facilitate financing for domestic production and advance all downstream technologies of rare earth products (Ernst and Young, 2010).

Contrary to their name, REE are relatively common in the earth's crust and have been known to exist in over 200 minerals, where any one of the REE can substitute for the major ion. The primary challenge lies in locating them in high enough concentrations with favourable mineralogical characteristics and elemental distributions to allow for profitable extraction. Bringing a potentially viable project into production can be particularly difficult when considering the immense amount of risk that must be considered to locate, finance and develop a REE operation. One of the primary sources of risk is the geological uncertainty of REE deposits or, more specifically, the uncertainty in material grades, tonnages, mineralogy and geology. The failure to properly address these geological risks may cause a project to fall short of expectations, which can be catastrophic for a mining business (Vallée, 2000). The focus of this paper will be the effective assessment and integration of these risks when developing a mine production schedule that will result in more realistic forecasts and allow for more informed engineering and business decisions.

The goal when developing a long-term, optimal mine production schedule is to define the most profitable extraction sequence of material in a deposit throughout the life of mine (LOM). This schedule dictates the annual metal outputs and cash flows and is, therefore, critical in accurately valuing a project to attract investors. Production scheduling is typically formulated as a mixed integer program (MIP) where the sequence and destination of extracted mining units known as “blocks” are modelled as binary decision variables contributing to some objective function while abiding by a series of operational constraints. Early works are successful in using exact methods to find the optimal solution to the mine production scheduling problem (Gershon, 1983; Caccetta and Hill, 2003; Ramazan and Dimitrakopoulos, 2004; Bley et al., 2010). However, all of these applications are limited threefold: they can be computationally intractable when scaled to a realistic problem size; they are usually only implementable in the simple case when the problem is linear and convex; and, most importantly, they all rely on a single deterministic representation of the orebody. The grade values in these conventional orebody models are often estimated using some type of weighted average of all surrounding sampled points (Isaaks and Srivastava, 1989). These estimation approaches, by construction, assign values to unknown locations that minimize the global variance of the deposit. The failure to represent the in-situ grade variability inevitably leads to the production target deviations mentioned above. The geostatistical approach known as stochastic spatial simulation, offers the capacity to model these uncertainties through the generation of multiple, equiprobable realizations of the deposit (Journel, 1979; Goovaerts, 1997). Unfortunately, there is no commercially available software that can develop mine production schedules that consider geological uncertainty using simulated orebodies. Dimitrakopoulos et al. (2007) assess the risk and reward of multiple schedules, created using independent stochastic simulations, as criteria to choose the best mine design. Godoy and Dimitrakopoulos (2004) use multiple mining schedules as input to develop one risk-resilient schedule using an approach based on simulated annealing. Dimitrakopoulos and Ramazan (2004) and Dimitrakopoulos and Grieco (2009) use a probabilistic measure to discourage the mining of blocks with a high likelihood of being below a cut-off grade. These sequential and probabilistic approaches have since been deemed ineffective in finding the truly optimal solution when considering geological uncertainty. Ramazan and Dimitrakopoulos (2013) propose an approach based on two-stage stochastic programming (Birge and Louveaux, 1997) to develop a mine production schedule robust to uncertainty. Results show significant improvement over conventional optimization practice by increasing the expected NPV while decreasing the risk of not meeting production targets. One major shortfall of this approach, and many before it, is that all material destinations must be determined prior to optimization. Menabde et al. (2007) devise a method that allots material into

discrete grade “bins”. The resulting optimization decides the associated ore or waste allocation of these bins which allows for a cut-off grade policy that can vary over time. The effectiveness of these approaches that rely on exact mathematical programming solving techniques are still limited by the size of the problem, and the reliance on the convexity of the solution space. This can be overcome by using an inexact class of methods to solve integer programs known as metaheuristics. By intelligently exploring a large, complex solution space, these algorithms have shown to find very high quality solutions to the mine production scheduling problem in reasonable amounts of time (Goodfellow and Dimitrakopoulos, 2014; Lamghari et al., 2014; Montiel and Dimitrakopoulos, 2014; Senécal and Dimitrakopoulos, 2014). In addition, the construction of these methods allows for the efficient solving of non-linear and non-convex problems caused when stockpiling and non-linear recovery functions are introduced.

For these stochastic mine planning approaches to be effective, it is imperative to generate high quality realizations of the deposit. Like most other commodities, the common practice to model REE deposits begins by assaying a drilling program for each of the metals of interest. This information is used to inform the remainder of the deposit which is bounded by some geological domain. Logically, the final representation of the deposit is very sensitive to the methods that describe the final extents of the domain, as well as the approach used to interpolate the material grades. To assess the uncertainty surrounding both of these aspects of geological modelling, a two-step simulation approach (Goodfellow et al., 2012) is used. First, the geological boundaries of the deposit are simulated. Traditionally, orebody boundaries are created using some attribute from the sampled data to trace the outlines of the material domains; this can capture the large-scale trends, but will be locally inaccurate, and thus will result in a subjective, overly-smoothed interpretation of the mineralized zones (Journel, 2007). Simulating the boundaries of geological domains allows for the quantification of the uncertainty involved. However, modelling algorithms that only consider two-point spatial statistics, fail to reproduce complex curvilinear patterns present in a naturally occurring deposit (Guardiano and Srivastava, 1993). Simulation algorithms that simultaneously consider multiple points can offer a more realistic reproduction of geological boundaries. The technique known as single normal equation simulation (SNESIM) (Strebelle, 2002; Boucher, 2009) is implemented to simulate the extents of the mineralization of a REE deposit. The second step consists of assessing the uncertainty about the spatial continuity of metal grades. Due to the strong correlations between REE of similar atomic size, it is imperative to respect and reproduce these naturally occurring cross-elemental relationships. Joint conditional simulation methods can be used to quantify the uncertainty surrounding the geospatial relationships of correlated variables. However, when dealing with larger deposits containing three or more correlated variables, these methods become overly complex to model and computationally intractable to implement. An alternative approach is applied that aims to decompose a set of correlated variables into uncorrelated 'factors'. The geostatistical application of this approach, based on principle component analysis (PCA) (David, 1988; Goovaerts, 1993; Wackernagel, 2003), is limited as it only guarantees decorrelation at a lag distance of zero. Alternatively, minimum/maximum autocorrelation factors (MAF) (Switzer and Green, 1984; Desbarats and Dimitrakopoulos, 2000; Boucher and Dimitrakopoulos, 2009) transforms the original variables into a set of orthogonal factors that are decorrelated at all lag distances. These factors are then simulated independently and back-transformed to the initial variable space, preserving the original spatial relationships.

This paper explores the process of simulating REE deposits and optimizing the annual production schedule while integrating geological uncertainty using a multi-element SIP formulation with flexible destination decisions. First, the conventional and stochastic approaches to modelling REE deposits are reviewed. The formulation of the SIP is introduced followed by the optimization procedure using a multi-neighbourhood tabu search metaheuristic (Lamghari and Dimitrakopoulos, 2012; Senécal and Dimitrakopoulos, 2014). This stochastic modelling and optimization approach is then applied to case study at an open pit, monazitic REE operation. This approach is benchmarked against the best-known conventional practices to demonstrate the advantages of designing a mine production schedule that integrates geological uncertainty.

2 Modelling REE deposits

2.1 Conventional approach

There has been very little published in terms of how to effectively model REE deposits and even less in terms of mine optimization. This is in part due to the fact that there are only a handful of REE focused projects currently operating around the world. Like most other commodities, the common practice is to assume fixed boundaries of geological domains to act as the extents of some estimation technique for the metal grades contained within. However, since every

REE deposit contains all of the REEs in varying concentrations, it can be tedious to model each of them, given that they are strongly correlated (Figure 1). One particular convention widely used in the REE industry is the use of a cumulative representation of ore quality known as the total rare earth oxide (TREO) grade. This simplified grade is derived from a weighted summation of the individual REE in a sample as seen in Eq. (1). The material grades of the deposit are typically estimated using this TREO grade which has major ramifications throughout the later processes of mine optimization. The primary drawback of using this convention is that the locations and magnitudes of the less concentrated, and more valuable, REE are lost due to their smaller contribution to the TREO grade. This loss of resolution leads to a misguided understanding of the eventual optimal production schedule, cut-off grade and final valuation, indicating that this convention should be avoided all together. For REE producers that aim to mine and sell their product as a bulk ore concentrate at a fixed TREO basket price, this approach may suffice, however, for producers that require a finer granularity to either accurately declare their reserves or forecast the production of individual REEs to achieve a strict blend, it is necessary to improve how the ore body is modelled.

$$TREO = \sum_{e \in REE} REEGrade_e \cdot OxideWeight_e \tag{1}$$

Extensions of this cumulative grade representation might be the separation of rare earths in various classes to group the elemental distribution according to similar properties, similar abundancy, and subsequently, similar market value. One of the more common groupings involves splitting the light rare earth elements (LREE), consisting of lanthanum to samarium, from the remaining heavy rare earth elements (HREE), europium to lutetium. Whether the TREO grade (Commerce Resources Corp, 2012; IAMGOLD, 2012; Molycorp Inc, 2012) or these groupings (Matamec, 2013) are used to estimate the grades of the orebody, both approaches will inevitably require some linear scaling to eventually assess individual REE content to forecast reserves. Unfortunately, scaling naturally infers perfect correlation which is known to be untrue. Another common approach to grade interpolation is to independently estimate each of the REE (Avalon Rare Metals Inc., 2013; Quest Rare Minerals Ltd., 2014; Great Western Minerals Group Ltd., 2014). Since all REEs in the sample data are highly correlated, by construction, an estimation technique will be sufficient in reproducing the cross relationships assuming that the each REEs spatial statistics do not vary drastically. Although it is an improvement over the grouping and scaling methods, any estimation technique will ignore the in-situ variability of grades throughout the deposit. Because of this, it should be sought to perform a joint conditional simulation to model the grades of all REE in a deposit. The following sections will cover the algorithms necessary to implement the two step stochastic simulation approach to model the volumetric and grade uncertainties pertaining to any typical REE deposit.

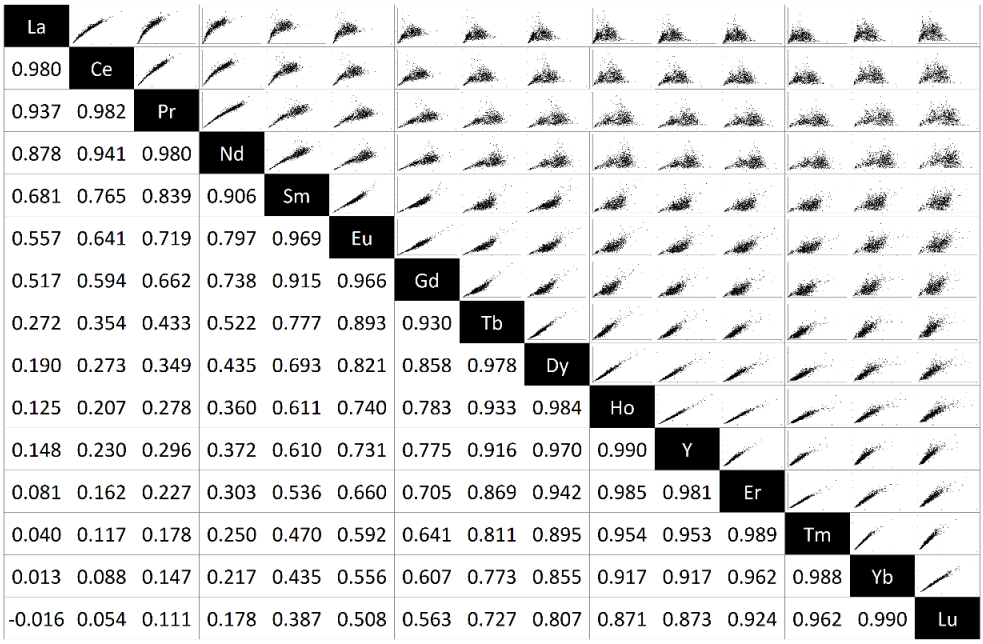

Figure 1: Cross plots (upper-diagonal) and Pearson correlation coefficients (lower-diagonal) of sampled REE grades

2.2 Multiple point simulation with single normal equation simulation

Multiple point (MP) statistics consider the joint neighbourhood of n surrounding points, centered around a location $\mathbf{x}_0$, referred herein as a template, τ_n, which is defined by a set of vectors, $\mathbf{h}_\alpha$, $\alpha \in \{1,...,n\}$. The realization of the n values within the template is known as a data event, $\mathbf{d}_n$, and these values are represented by an attribute s taking on one of K possible discrete states. These states will likely represent types of lithologies or metallurgical ore types. An example of a data event on a template of size $n = 4$ can be seen in Figure 2. A brief outline of the SNESIM algorithm can be found below and a more detailed explanation can be found in Guardiano and Srivastava (1993) and Strebelle (2002).

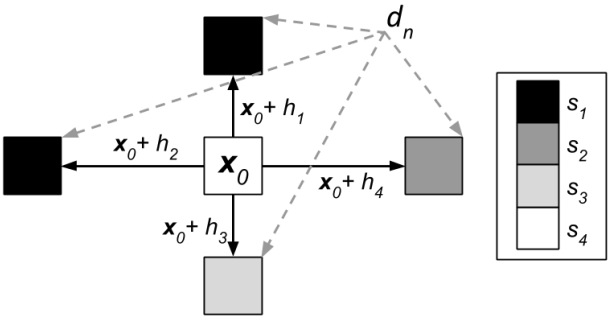

Figure 2: Configuration of a data event. Conditioning points centered on location $\mathbf{x}_0$

General algorithm steps:

1. Scan the training image and store all occurrences of all data events.
2. Define a random path to visit each node to be simulated.
3. For each node in the random path:
    a. Retrieve all stored data events that contain the surrounding conditioning data and previously simulated nodes.
    b. Derive the local probability distribution from stored frequencies of central values. The probability of finding a certain categorical state given the surrounding data event is given by the Bayes' relation for conditional probability.
    c. Randomly sample the conditional cumulative distribution function to select a pattern and add the now simulated node to the grid.
4. Repeat all previous steps for the desired amount of realizations.

2.3 Joint simulation using minimum/maximum autocorrelation factors

Let $\mathbf{Z}(\mathbf{x}) = \left[z_1(\mathbf{x}),..., z_p(\mathbf{x}) \right]^T$ denote a multivariate, stationary and ergodic random field over a region, representing p correlated, continuous variables. Now consider its point-wise standard Gaussian transformation, $y_i(\mathbf{x}) = \varphi\left(z_i(\mathbf{x}) \right)$, to have zero mean and unit variance:

$$\mathbf{Y}(\mathbf{x}) = \left[y_1(\mathbf{x}),..., y_p(\mathbf{x}) \right]^T \tag{2}$$

The decorrelation at lag zero is achieved by generating the PCA factors $\mathbf{F}_{PCA}(\mathbf{x})$:

$$\mathbf{F}_{PCA}(\mathbf{x}) = \Lambda_1^{-1/2} \mathbf{Q}_1 \mathbf{Y}(\mathbf{x}) \tag{3}$$

Where $\mathbf{\Lambda}_1$ and $\mathbf{Q}_1$ are from the spectral decomposition of the covariance matrix $\mathbf{B}$, of $\mathbf{Y}(\mathbf{x})$

$$\mathbf{B} = \mathbf{Q}_1^T \mathbf{\Lambda}_1 \mathbf{Q}_1 \tag{4}$$

To ensure the spatial decorrelation at all lag distances, we apply a second data transformation:

$$\mathbf{F}_{MAF}(\mathbf{x}) = \mathbf{Q}_2 \mathbf{F}_{PCA}(\mathbf{x}) \tag{5}$$

Where $\mathbf{Q}_2$ is derived from the spectral decomposition of the experimental cross-covariance matrix $\mathbf{\Gamma}(\Delta)$, of $\mathbf{F}_{PCA}(\mathbf{x})$, given some experimental lag distance Δ.

$$\mathbf{\Gamma}(\Delta) = \mathbf{Q}_2^T \mathbf{\Lambda}_2 \mathbf{Q}_2 \tag{6}$$

In this data-driven decorrelation approach (Rondon, 2012), it is common to test many values of Δ, and select the one that yields the best decorrelation. The minimum/maximum autocorrelation factors (MAF) in Eq. 5 are, by definition, spatially uncorrelated at all lag distances (Desbarats and Dimitrakopoulos, 2000) and each factor can be simulated independently. Furthermore, since the factors are assumed to be normally distributed, any efficient sequential Gaussian simulation method can be utilized (Goovaerts, 1997; Dimitrakopoulos and Luo, 2004). In this work, a computationally efficient method known as direct block simulation (DBSim) (Godoy, 2003) is used. A more detailed description of the decorrelation procedure and the integration with DBSim can be found in Boucher and Dimitrakopoulos (2009).

General algorithm steps:

1. Transform the data $\mathbf{Z}(\mathbf{x})$ to normal scores $\mathbf{Y}(\mathbf{x})$.
2. Orthogonalize $\mathbf{Y}(\mathbf{x})$ using MAF transformation to obtain $\mathbf{F}_{MAF}(\mathbf{x})$.
3. Define a random path visiting each block to be simulated.
4. For each block in the random path:
    a. Define a random path visiting each point in the block.
    b. Simulate each of the factors at each point.
    c. For each factor, take the average of all points within the block to include in further conditioning in the MAF space.
    d. Back-transform the simulated points for all factors to the original data space and re-block in order to obtain the simulated block values.
5. Repeat steps 3 - 5 for the desired number of simulations.

3 Stochastic optimization of open pit mine production scheduling

3.1 Stochastic integer programming formulation

The following two-stage stochastic recourse model offers a means to solve the open pit mine production scheduling problem (OPMPSP) with uncertain geology. In general, this-two stage approach is a type of stochastic programming model that integrates both anticipative and adaptive mechanisms of dealing with uncertain input. First stage, or anticipative decisions, involve making decisions prior to the unveiling of uncertainty, whereas second stage, or adaptive decisions, are made once uncertain parameters have been observed. In mining terms, this can be thought of as making extraction sequence decisions independent of scenario, whereas the risk of deviating from production targets can be controlled on a per-scenario basis acting as a corrective strategy (Dimitrakopoulos and Ramazan, 2008).

The first stage decisions that are to be solved in this formulation are when blocks should be extracted and where they should be sent. The latter decisions are particularly useful when considering a complex, multi-element deposit. All elements have unique concentrations, market values and associated operational constraints. These added complexities make it substantially more difficult to derive a multi-element cut-off grade policy. Informing the optimizer with: the uncertainty about the grades of each element in a block, the various blending requirements, and the

state of the mining and processing capacities, allows for the derivation of a more robust destination policy. The following SIP formulation is based on the model introduced in Ramazan and Dimitrakopoulos (2013) with modifications necessary to expand the problem to a multi-element operation.

Sets and indices

N	number of blocks considered in the deposit
i	block index, $i \in 1,...,N$
T	number of periods considered in the life of mine
t	period index, $t \in 1,...,T$
P	number of processing destinations considered
p	material destination index, $p \in 1,...,P$
E	number of elements considered
e	element index, $e \in 1,...,E$
S	number of ore body scenarios considered
s	scenario index, $s \in 1,...,S$

Constants

O_i	set of blocks that overly block i
m_i	mass of block i
g_{ies}	grade of element e in block i in scenario s
d_f	financial discount rate, $d_f \in [0,1]$
d_g	geological discount rate, $d_g \in [0,1]$
MC_i	cost to mine block i
PC_{ip}	cost to process block i at destination p
r_{pe}	recovery of element e at destination p
π_e	selling price of element e
$\alpha_{ipts} = \frac{\left(\sum_{e=1}^{E} m_i \cdot g_{ies} \cdot r_{pe} \cdot \pi_e\right) - PC_{ip}}{(1+d_f)^t}$	discounted profit generated by processing block i at destination p in period t in scenario s
$\beta_{it} = \frac{m_i \cdot MC_i}{(1+d_f)^t}$	discounted cost of mining block i in period t
$C_{pt}^{\pm} = \frac{C_p^{\pm}}{\left(1+d_g\right)^t}$	discounted cost per unit shortage/surplus being sent to destination p in period t. Also used to represent discounted cost per unit shortage/surplus of element e if indexed accordingly.
M_t^{cap}	maximum capacity for tonnage mined in period t
O_{pt}^{tar}	target for tonnage of ore processed at destination p in period t
G_{pet}^{tar}	target material grade for element e at destination p in period t

Variables

$x_{it} = \begin{cases} 1 \\ 0 \end{cases}$.	if block *i* is mined during period *t*, otherwise
$y_{ipt} = \begin{cases} 1 \\ 0 \end{cases}$.	if block *i* is processed at destination *p* during period *t*, otherwise

d^-_{pts}, d^+_{pts}	shortage/surplus deviations for the tonnage processed at destination p in period t for scenario s.
d^-_{pets}, d^+_{pets}	shortage and surplus grade deviations for element e at destination p in period t for scenario s.

Objective function:

$$\text{Max: } \sum_{t=1}^{T}\left\{\underbrace{\sum_{i=1}^{N}\left\{\frac{1}{S}\sum_{s=1}^{S}\sum_{p=1}^{P}\left\{\alpha_{ipts}\cdot y_{ipt}\right\}-\beta_{it}\cdot x_{it}\right\}}_{\text{Part 1}} - \underbrace{\sum_{p=1}^{P}\sum_{s=1}^{S}\left\{C^-_{pt}\cdot d^-_{pts}+C^+_{pt}\cdot d^+_{pts}+\sum_{e=1}^{E}\left\{C^-_{pet}\cdot d^-_{pets}+C^+_{pet}\cdot d^+_{pets}\right\}\right\}}_{\text{Part 2}}\right\} \tag{7}$$

The objective function of this SIP model aims to maximize the difference between the expected profits and the costs of deviating from planned production targets. Part 1 refers to the total expected discounted cash flows from mining and processing material. The second part adds the geological risk management parameters. Notice that all deviations cost parameters are indexed by time. By discounting these costs across the time series, the optimizer is encouraged to defer risk later into the project life where it is assumed that corrections can be made. This mechanism is known as geological discounting. Part 2 accounts for both the costs associated with deviating from ore tonnage targets and the costs of deviating from grade targets at each destination.

Subject to:

Extraction and processing linkage constraints ensure that a block must be extracted before it is sent to any destination.

$$\sum_{p=1}^{P} y_{ipt} = x_{it} \qquad \forall i,t \tag{8}$$

Reserve constraints ensure that a block can only be extracted once throughout the LOM.

$$\sum_{t=1}^{T} x_{it} \le 1 \qquad \forall i \tag{9}$$

Precedence constraints inform the model that in order to extract any block, all the overlying blocks must be extracted first.

$$x_{it} \le \sum_{\tau=1}^{t} x_{j\tau} \qquad \forall i,t,\ j \in O_i \tag{10}$$

Mining capacity constraints ensure that the mining capacity is not violated

$$\sum_{i=1}^{N} m_i \cdot x_{it} \le M_t^{cap} \qquad \forall t \tag{11}$$

Ore processing constraints are used to determine the shortage and surplus tonnages from the production targets

$$\sum_{i=1}^{N} m_i \cdot y_{ipt} - d^+_{pts} + d^-_{pts} = O^{tar}_{pt} \qquad \forall p,t,s \tag{12}$$

Grade blending constraints are used to determine the deviations above or below the grade production targets at each processing destinations.

$$\sum_{i=1}^{N}\left(g_{ies}-G_{pet}^{tar}\right)\cdot y_{ipt}-d_{pets}^{+}+d_{pets}^{-}=0 \qquad \forall p,e,t,s \tag{13}$$

Variable bounds.

$$x_{it}\in\{0,1\} \qquad \forall i,t \tag{14}$$

$$y_{ipt}\in\{0,1\} \qquad \forall i,\ p,t \tag{15}$$

$$d_{pts}^{+},\ d_{pts}^{-}\geq 0 \qquad \forall p,t,s \tag{16}$$

$$d_{pets}^{+},\ d_{pets}^{-}\geq 0 \qquad \forall p,e,t,s \tag{17}$$

4 Solution approach: Multi-neighbourhood tabu search

When the OPMPSP approaches realistic problem sizes, conventional mathematical programming solvers become less viable options due to their prolonged solving times. For this reason, inexact methods of solving large integer programs known as metaheuristics are implemented. The multi-neighbourhood tabu search method (MNTS) (Glover and Laguna, 1997; Lamghari and Dimitrakopoulos, 2012; Senécal and Dimitrakopoulos, 2014) uses basic move operators to explore the feasible solution space to gradually improve the objective function of the proposed model. The two move operators consist of changing a blocks extraction period and changing a blocks destination.

Predefined combinations of these moves are defined as neighbourhoods of the current solution vector. There are four different neighbourhoods considered in this case: changing a blocks extraction period without violating precedence, changing a blocks destination, changing a blocks destination and extraction period without violating precedence and swapping the destinations of two blocks extracted in the same period. At each iteration, all four neighbourhoods are explored and the neighbour that results in the best improvement to the objective function is selected and the solution vector is updated. The most important feature of this solving method is what is referred to as the tabu list. A list of previously explored neighbours is kept in memory which are to be removed, or rendered '*tabu*', from consideration at the succeeding iterations. These tabu moves allow the solver to avoid cycling and to escape local optima. Other mechanisms are also implemented to reduce the amount of unlikely neighbours considered to improve the efficiency of the solver.

5 Case study – Jupiter deposit

To demonstrate the effectiveness of methods described herein, an application is carried out at a fictitious REE operation known as the Jupiter mine. The following section will cover the two-step simulation of the Jupiter deposit followed by the stochastic optimization of the mine production schedule.

5.1 Jupiter simulation

The features of the Jupiter orebody are based on a real, greenfield REE deposit which will remain undisclosed for confidentiality purposes. The deposit's geometry and geology can be described as a steeply North-dipping, massive ovoid measuring approximately 700 m along strike, 500 m across and reaching depths of over 650 m. The deposit is predominantly abundant in LREE with an area of higher HREE concentration hosted near the surface, covered by a very thin layer of overburden. Almost all of the deposit's REEs are hosted by monazite and bastnäsite, which are two of the most common and historically exploitable REE bearing minerals. The data used for this study is comprised of 21 exploration drill holes, spaced approximately 50 m apart, containing 7,836 core samples at an average length of 0.93 m. The majority of the drill holes are vertical in direction with some of the shorter holes dipping at roughly 45 degrees on an Eastern strike. The samples are assayed for yttrium and 14 of the 15 lanthanide elements; lanthanum, cerium, praseodymium, neodymium, samarium, europium, gadolinium, terbium, dysprosium, holmium, erbium,

thulium, ytterbium and lutetium. In addition, the ratio of monazite to bastnäsite is also assessed throughout the deposit. This ratio is not provided in the data set but is deemed critical for optimization purposes as will be discussed later. The necessary conditioning information for the mineral ratio is generated on a sparse, uniform grid by randomly sampling a log-normal distribution and scaling the values to follow the trends of cerium. For this application, this approach is deemed sufficient in replicating the spatial relationships of this naturally occurring phenomena. Twenty geological domain simulations are generated using SNESIM and each one acts as the unique extents of one joint conditional simulation of REE grades using MAF. The simulation of the monazite-bastnäsite ratio is done independently using sequential indicator simulation (SIS).

5.1.1 Simulation of geological boundaries

A traditional wireframe serves as a training image to encompass the large scale geometric shapes and features of the deposit. This TI is generated by first coding the 7,836 borehole samples as inside or outside the interpreted domain. The envelope is traced and converted to a block model on a regular grid where all blocks lying within the wireframe are considered to be mineralized, and blocks lying outside are considered to be barren rock. The SNESIM algorithm is implemented given the coded borehole samples as conditioning data on point support and the block model as the training image. The simulation grid measures 630, 850 and 840 m in the East-West, North-South and vertical directions respectively and the grid is discretized by blocks measuring 10 x 10 x 10 m. The massive nature of the deposit allows for relatively consistent and simple patterns about the boundary of the domain, thus, the reproduction of the simulations are relatively similar in terms of their total volume. The distribution of the simulated volumes can be seen in Figure 3. The results show that approximately 40% of the simulations are larger than the training image and 60% are smaller in terms of total mineralized volume. Figure 4 compares the cross sections of the TI to the smallest, median, and largest domain simulations after applying post-processing to remove erroneous mineralized blocks from the outer corners of the simulation grid. The large scale features of the training image are preserved, however, the simulated domains show the presence of spatial variability at the local scale. After quantifying the volumetric uncertainty in the mineralized domain, the uncertainty pertaining to spatial continuity of REE grades can be assessed by performing a joint conditional simulation within each of these domain realizations using MAF.

5.1.2 Simulation of REE grades

The 3 m samples are declustered to remove any bias introduced by concentrating drilling in areas of higher grades which is not uncommon in most exploration programs. The conditioning points are independently filtered through each of the domain simulations resulting in twenty unique input data sets. In this case, the REE grades are partitioned into three segments. The LREE, MREE and HREE are treated independently to simplify the decorrelation process and the eventual validation steps without compromising the most prevalent relationships. It is noted that this simulation approach is not limited by the amount of variables considered, as long as the decorrelation is deemed satisfactory. It is encouraged to jointly simulate all of the REE together for the most accurate representation of the orebody, but this segmented approach will suffice for this application. Following a normal score transformation of the conditioning data, an experimental lag distance of 75 ± 35 m is used to ensure adequate decorrelation. An example cross-variogram of two of the LREE service factors can be seen in Figure 5. Notice the proximity to zero suggesting that these factors are well-decorrelated at all lag distances.

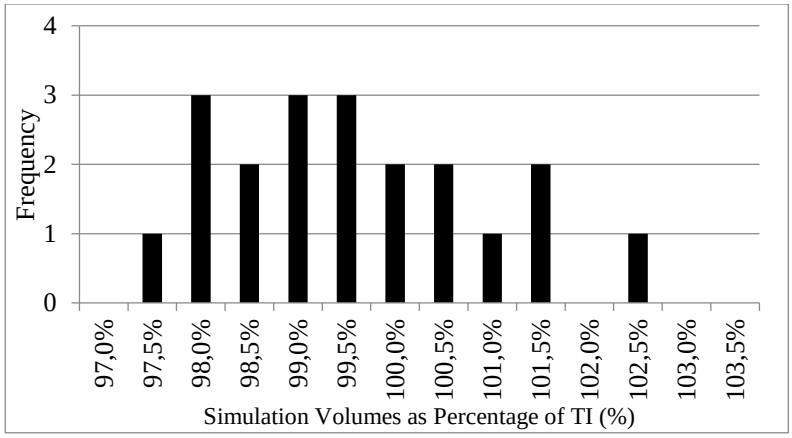

Figure 3: Frequency distribution of simulated mineralized volumes expressed as percentage of the training image

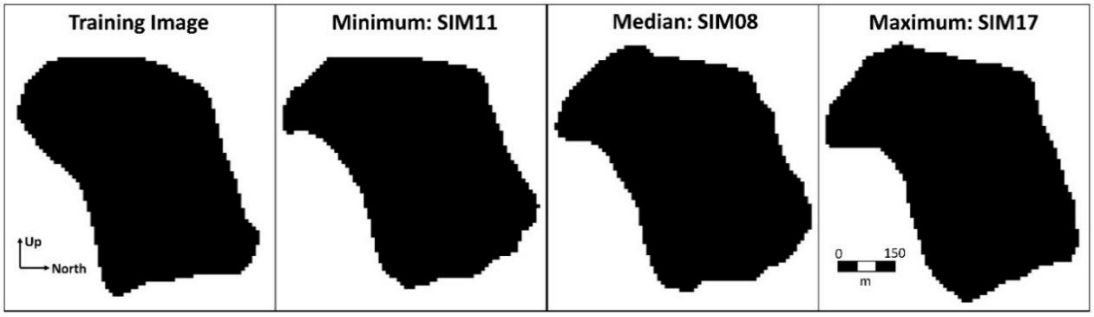

Figure 4: Vertical cross-sections of the training image, and the minimum, median and maximum ore domain simulations

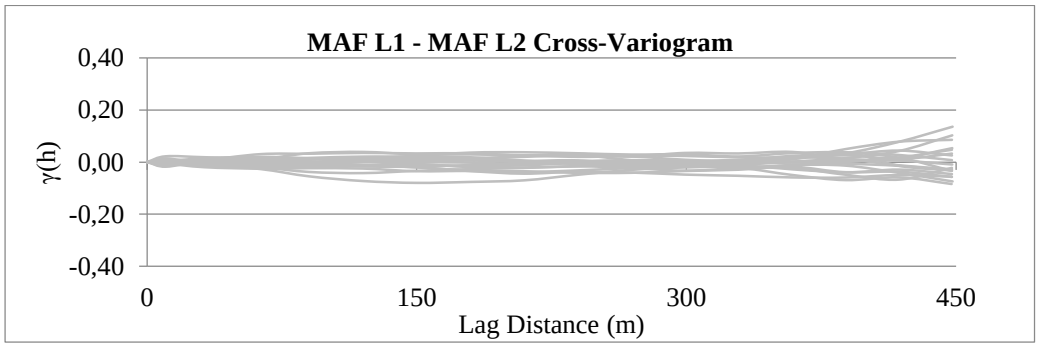

Figure 5: Cross-variogram of MAF light factors 1 and 2

Direct block simulation is performed on each of the service factors at a node discretization of 5 x 5 x 5 m. Due to the varying extents of the mineralized zones from the previous step, the amount of simulated nodes varies between 633,472 and 660,536. The appropriate back-transformation is applied to the simulated factors to yield the final simulated points in the original data space. The simulated LREE, MREE and HREE values are combined and re-blocked to produce the final simulations. Figure 6, Figure 7 and Figure 8 validate the spatial continuity of the conditional simulations with histograms, variograms and cross-variograms. The black line represents the original data, filtered through the median orebody, and the light grey lines represent the simulations on point support randomly sampled at 2%.

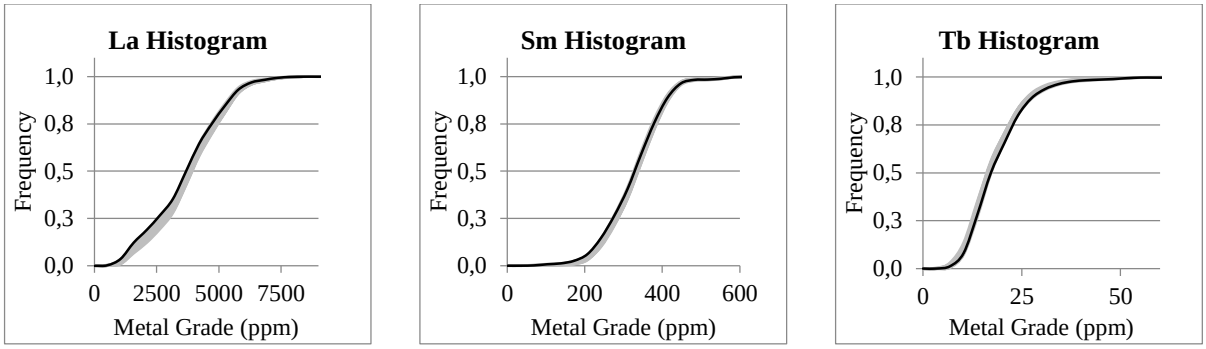

Figure 6: Histograms for lanthanum, samarium and terbium grades

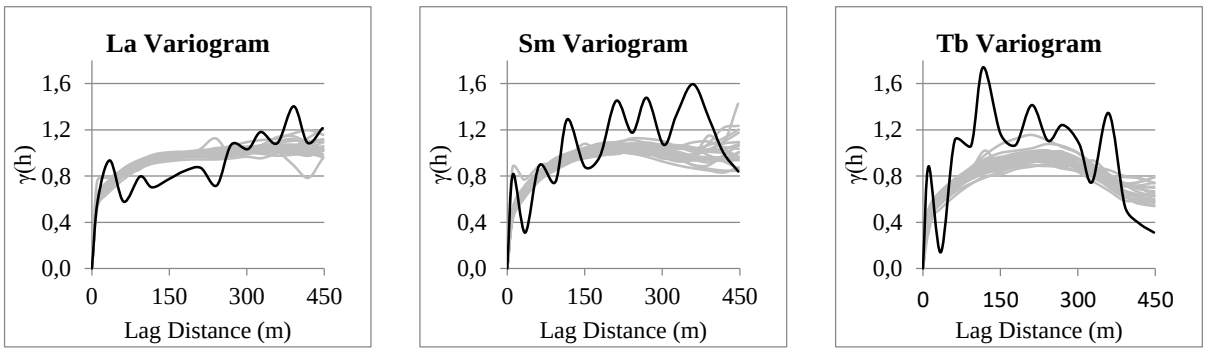

Figure 7: Standardized variograms for lanthanum, samarium and terbium

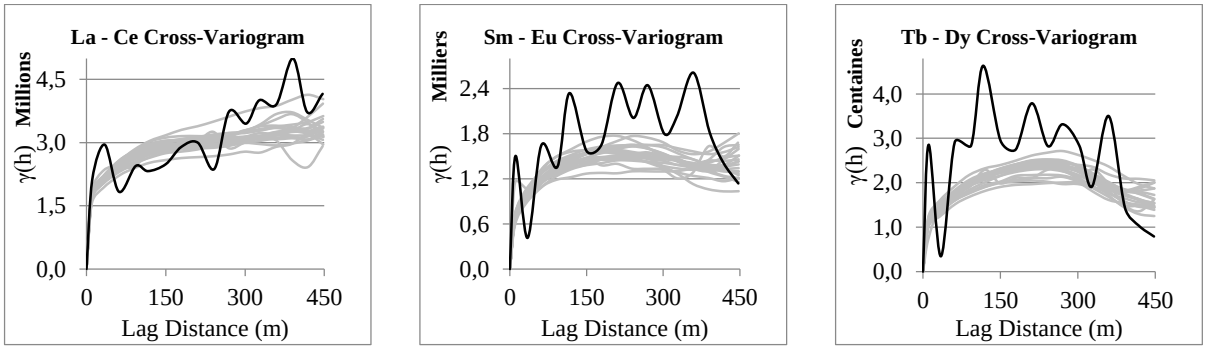

Figure 8: Cross-variograms for lanthanum and cerium, samarium and europium and terbium and dysprosium

The statistical validation demonstrates that the simulation is successful in reproducing the univariate and bivariate relationships of the conditioning information. It should be noted that the conditioning data is relatively sparse in terms of pairings found, which results in its sporadic nature. Figure 9 demonstrates the varying spatial continuity of grades between different simulations. The warmer colours represent higher grades for dysprosium across three example simulations. Figure 10 also assists in visually validating that the simulation approach is successful in reproducing the spatial cross-element relationships within one realization. The areas of concentrated high grades are similar amongst the LREE, lanthanum and cerium, however, once compared to the heavier element, dysprosium, the locations of the concentrated zones become dissimilar.

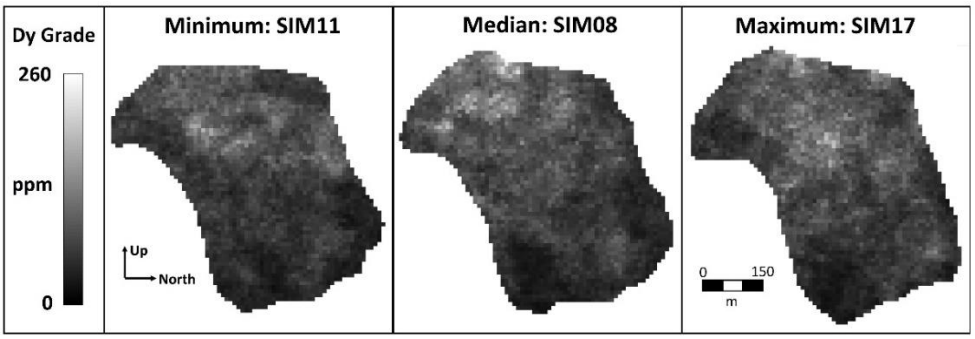

Figure 9: Simulated dysprosium grades across three different simulations

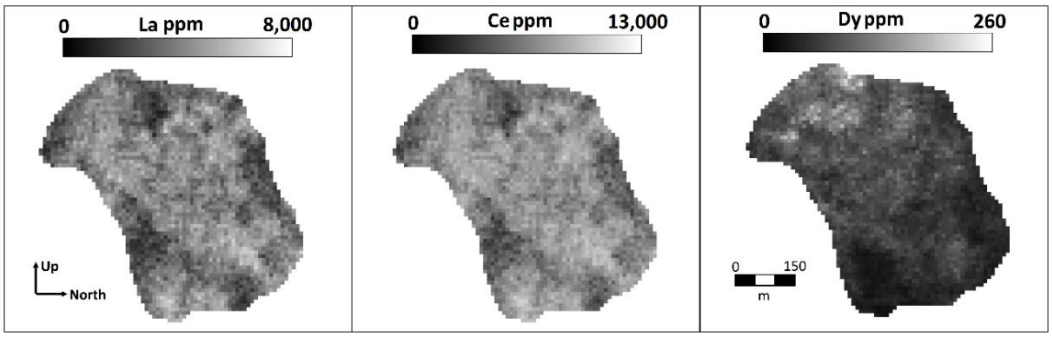

Figure 10: Simulated lanthanum, cerium and dysprosium grades within one simulation

5.2 Stochastic mine production schedule at the Jupiter deposit

The entire simulated resource model will require over 75 years to deplete, therefore, only the first 11 years of the LOM are scheduled to show the benefits of stochastic mine optimization. The truck-and-shovel, open-pit operation consists of one mine, and two destinations; a waste dump and one processing facility that produces four distinct, saleable REE products. The annual mining and processing rates are gradually increased throughout the first three years of operation to emulate fleet and plant expansions. The ore material delivered from the mine is crushed prior to flowing through a series of flotation cells to recover both monazite and bastnäsite. The flotation process has been designed to handle specific concentrations of both monazite and bastnäsite. To ensure optimal recovery, the run of mine (ROM) ore feed should fall within these designed grade ranges. The concentrate from this stage then moves to an acid 'cracking' step, where a bulk rare earth oxide solution is purified. The solution then flows through four sequential separation stages to produce the Jupiter products: a heavy and middle rare earth concentrate; a praseodymium and neodymium (didymium) mixture; a cerium product; and a lanthanum product. Each product stream has its own unique metal recovery. Once separated, the HREE and MREE product is sampled for its individual REE content and is sold accordingly. It is assumed that all of this product, along with the La and Ce products, can be sold in full at fixed prices. However, in this particular application, there is a very stringent offtake agreement with some customer purchasing the didymium product in order to produce didymium-iron-boron magnets. The agreement states that there are very tight requirements on the quantity of product that is purchased annually, and that the quality of the blend in terms of the ratio of Pr to Nd is to be heavily controlled. Breaching the terms of this agreement will result in various penalty fees.

The goals are to maximize the discounted value of the mine and to achieve the ore production targets while mitigating the risk that the mill feed deviates from the desired mineralogical concentrations and REE blend. This risk is quantified by using a set of twenty geological simulations. This stochastic approach to mine scheduling is bench marked against the best known conventional practices. This conventional schedule is generated using Geovia's Whittle 4X using an estimated ore body model as input. The original TI of the Jupiter deposit is used to bound the mineralized domain of this deterministic model, and each of the REE grades and the monazite-bastnäsite ratio are independently interpolated using ordinary kriging. The schedules will be compared using annual key performance indicators (KPI) such as NPV, annual tonnages mined and processed, and ROM mineralization and REE grades.

5.2.1 Optimization parameters

The annual grade targets for Pr and Nd are derived from the annual didymium production target of 24 thousand tonnes per year, the target ore production of 7 million tonnes per year and the desired Pr-Nd ratio of 78% Nd. It is observed that the annual mining rates and REE production tonnages are relatively high compared to currently operating mines, however, they could easily be scaled to more realistic numbers given that this data were available. The same holds true for the metal prices.

Table 1: Operation and financial parameters of the Jupiter mine

Parameter	Value	Parameter	Value
Periods	11 years	Monazite Range	2.1 – 2.3 %
Slope angle	45°	Bastnäsite Range	0.365 – 0.395 %
Blocks	106,487	Praseodymium Target	750 ppm
Density	2.98 t/m³	Neodymium Target	2,700 ppm
Mining capacity	20 – 35 Mt/year	Flotation recovery	70 %
Processing target	4.5 – 7.0 Mt/year	Cracking recovery	95 %
Financial discount	10 %	H+MREE recovery	92 %
Geological discount	20 %	Didymium recovery	95 %
Mining cost	6.50 $/t	Lanthanum recovery	93 %
Processing cost	112.00 $/t	Cerium recovery	91 %

Table 2: REE metal prices

Metal	Price $CAD/lb	Metal	Price $CAD/lb	Metal	Price $CAD/lb
Yttrium	16.20	Samarium	6.20	Holmium	320.00
Lanthanum	6.24	Europium	450.00	Erbium	275.00
Cerium	6.20	Gadolinium	25.00	Thulium	500.00
Praseodymium	60.60	Terbium	385.00	Ytterbium	360.00
Neodymium	72.80	Dysprosium	216.00	Lutetium	650.00

5.3 Stochastic results

The stochastic solution to the SIP formulation is found using the multi-neighbourhood tabu search on an Intel Xeon 5650 (2.67 GHz) with a total of 24 threads and 24 GB of RAM. A crude conventional schedule is used as an initial solution. The solver ran for approximately eight hours before deriving the final solution. Figure 11 shows a cross-section displaying the general progression of pit development. The schedule obeys all slope constraints and yields relatively mineable shapes that would require minor corrections to be operationally implementable. Since destinations are assumed to be fixed across all scenarios, the tonnages mined and processed will be consistent across all scenarios as seen in Figure 12 and Figure 13. Alternatively, the mineralization and REE blend will vary, and is shown using the individual light grey lines in Figure 14. Figure 12 shows that the total mining capacity is always honoured in the stochastic schedule and it could be argued that the planned fleet expansion could be modified and deferred to later in the LOM, given that the capacity is not fully exploited during the earlier periods. The schedule efficiently utilizes the processing capacity across all periods with the exception of year nine due to the large concentration of waste encountered in this area of the pit (Figure 13). In terms of the annual mineralization targets shown in Figure 14, the stochastic schedule is successful in controlling the ore feed within the optimized ranges over all geological scenarios. This ensures that the planned recovery at the flotation stage will have a strong likelihood of being realized, eventually leading to more metal and more revenue. Similarly, the Pr and Nd in the ore feed are expected to be within acceptable bounds of the targets throughout the mine life. This alludes that the didymium blend is suitable for the customer and that the correct quantity of product will be sold each year, resulting in little or no penalty costs. These results are useful in demonstrating the effects of geological discounting: the risk profiles are relatively tight in the earlier years of operation, indicating effective management of risk, whereas, the later years show a larger variation in REE grades. It is assumed that over time, more information will become available and corrective measures can be applied to reduce these risks that have been deferred to later years. Next, this stochastic schedule is bench marked against the conventional mine production schedule and comparisons are drawn.

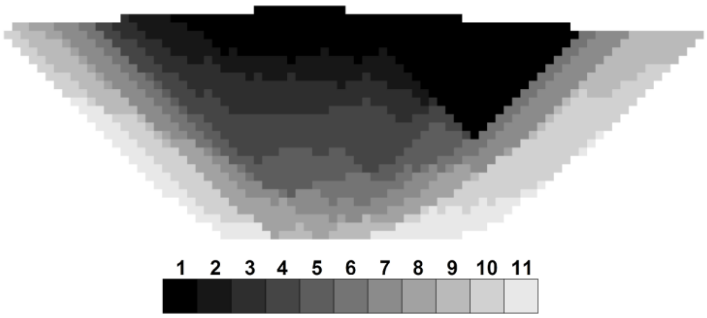

Figure 11: East-West cross-section of the stochastic schedule

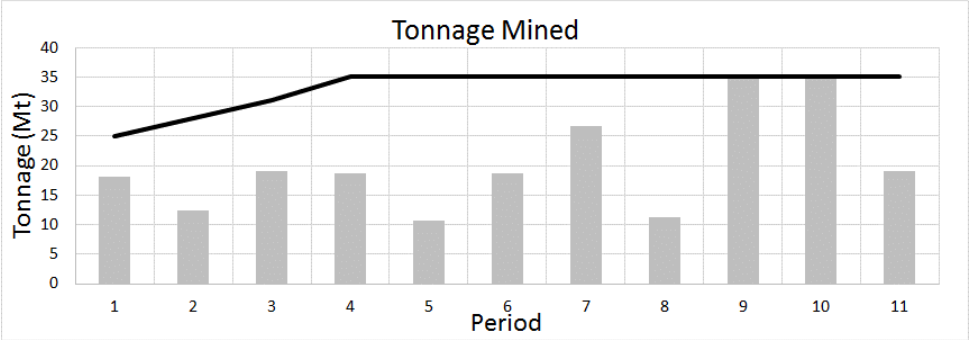

Figure 12: Annual tonnage mined for the stochastic schedule

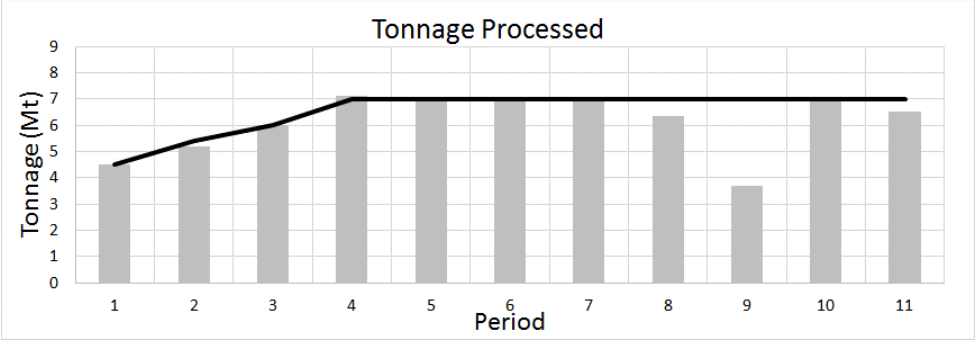

Figure 13: Annual tonnage processed for the stochastic schedule

5.4 Conventional results

This conventional schedule is developed using the same operational and financial parameters with the same objectives as the stochastic approach. Without the availability of extensive stockpiling, this solver relies on the flexibility of mining and processing fractions of blocks to meet the mineralization and REE blend requirements. Due to the tight nature of these targets, approximately 51% of the blocks are either partially mined or processed in the deterministic solution. It is necessary to make an approximation of this unrealistic schedule in order to provide a comparison to the stochastic solution. The simple rounding approximation outlines that blocks extracted in multiple periods are to be interpreted as fully mined in the period where the majority of the material is mined. Also, if less than half of a block is processed, that block is considered waste and vice versa for ore. A risk analysis can now be performed by running each geological simulation through the deterministic schedule. The LOM in this case is one year shorter than the stochastic approach. The final mining extents cannot be bounded directly by time using this particular solver. An ultimate pit limit is decided earlier in the optimization process by discretizing the space and using approximated

discounting, which is considered to be a suboptimal practice. The final conventional schedule is found to be 13 periods, however, since this study does not aim to determine the ultimate pit, the conventional schedule is trimmed to 11 years for a balanced comparison. The eleventh year of production yields negative cash flows and is therefore truncated from the solution to preserve optimism. The mining rate, shown in Figure 16, is violated in three periods, most notably, in the first and most critical year of production. This surplus mining will lead to inaccurate metal and cash forecasts since it will be impossible to mine the amount of material that the schedule is suggesting. The mining capacity is under-utilized in the remaining periods; these large fluctuations are most likely attributed to the need for an approximation of the partial extraction sequence generated by this solver.

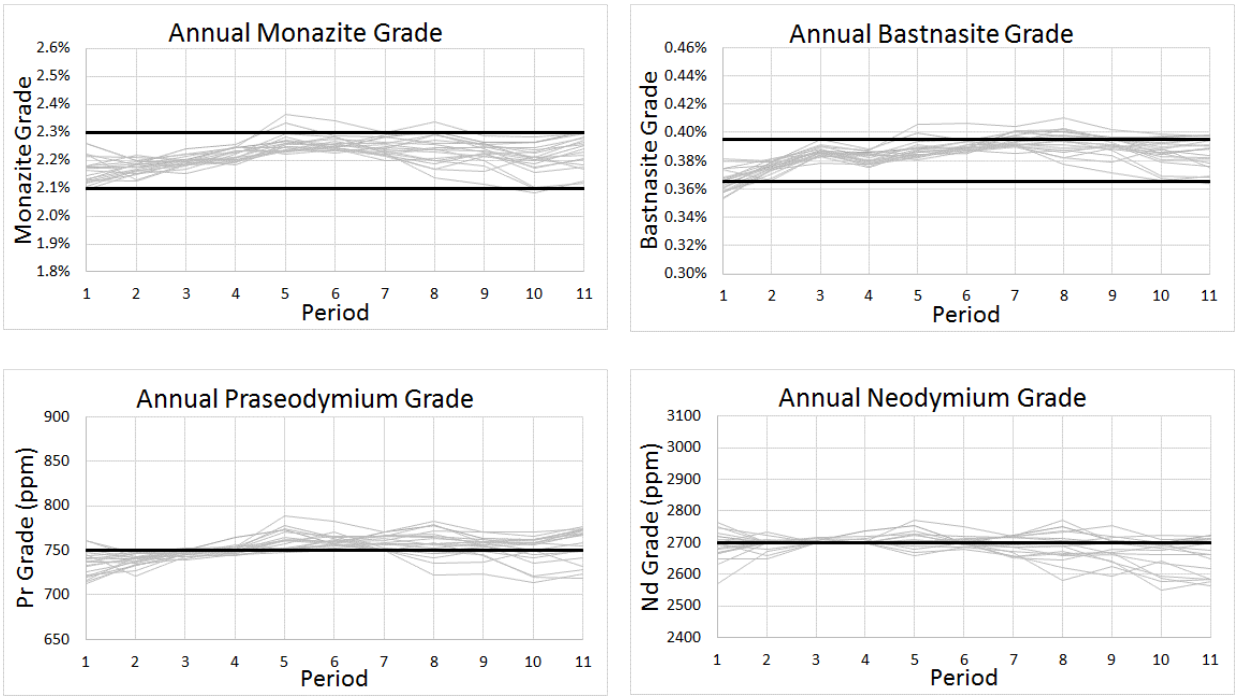

Figure 14: Annual mineralization and REE grades for the stochastic schedule. Monazite (top-left), bastnäsite (top-right), praseodymium (bottom-left) and neodymium (bottom-right)

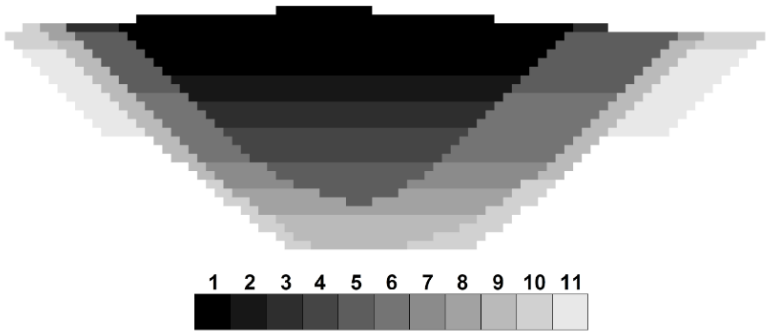

Figure 15: East-West cross-section of the conventional schedule

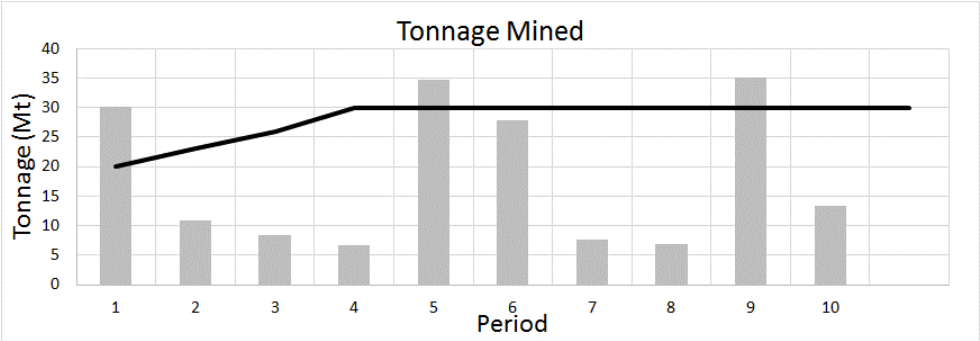

Figure 16: Annual tonnage mined for the conventional schedule

Figure 17 indicates that the processing capacity of the conventional schedule is not utilized as efficiently when compared to the stochastic solution. The limit is exceeded in two of the periods and the planned rate falls short of the target in the remaining eight. Regarding the mineralization and REE blend targets in Figure 18, the stochastic schedule out performs the conventional schedule; both in regards to meeting the targets with higher accuracy, but also with far more confidence, evidenced by the tighter risk profiles. It is unlikely that the mineral ratio of the ore feed delivered in the conventional schedule will fall within the optimal targets which will cause a substantial decrease in flotation recovery. It is also apparent that there is a very strong likelihood that penalty costs will be incurred due to the fluctuating quality of the didymium blend, as well as inventory costs of stockpiling unsold product in periods five, eight and nine. The final comparison between the two schedules is made via the projects LOM NPV in Figure 19. The NPV is described by the 10^{th}, 50^{th} and 90^{th} percentile of all scenarios, rather than each individually. The stochastic schedule yields an expected NPV increase of 20% over the conventional approach. It should also be noted that the final NPV of the conventional schedule does not incorporate the detrimental aspects just described. Due to early mining violations, the strong likelihood of decreased recoveries and penalty fees as per the offtake agreement, the deterministic cash flows in Figure 19 are misleading and will likely to be lower than demonstrated.

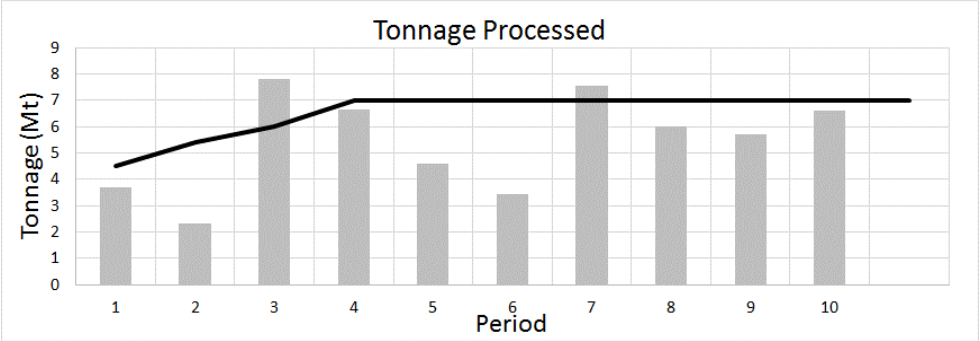

Figure 17: Annual tonnage processed for the conventional schedule

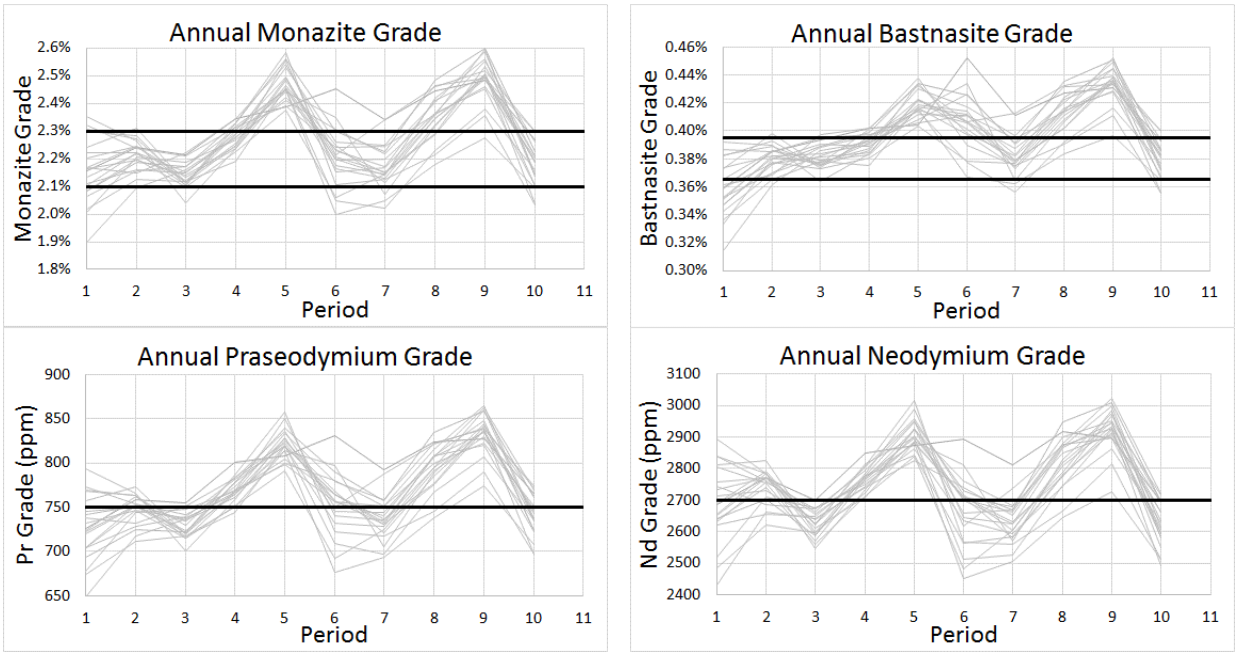

Figure 18: Annual mineralization and REE grades for the conventional schedule. Monazite (top-left), bastnäsite (top-right), praseodymium (bottom-left) and neodymium (bottom-right)

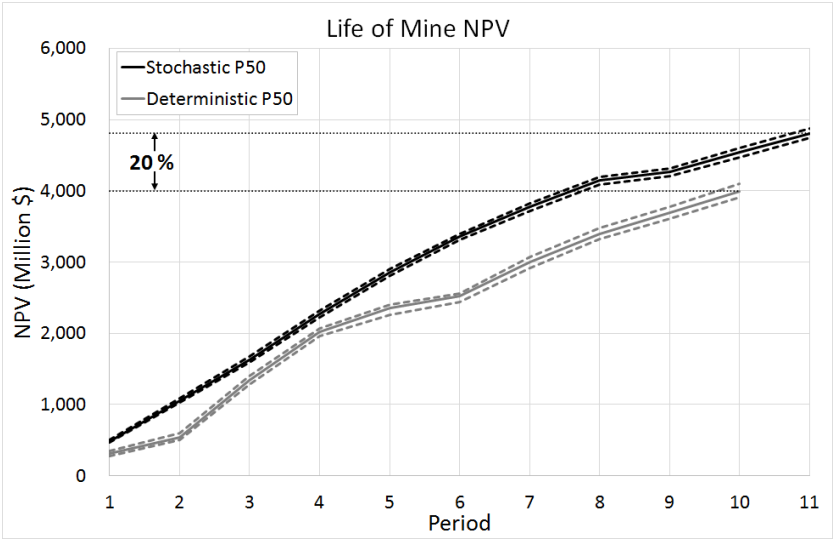

Figure 19: Cumulative NPV comparison between the stochastic schedule (black) and the conventional schedule (grey)

The results presented herein demonstrate the advantages that stochastic mine optimization can offer over the more conventional methods. By incorporating geological uncertainty into the optimization, logically, the risk of achieving certain production targets can then be explicitly controlled. However, it has also been shown that the expected value can also be significantly improved by adopting this risk-based scheduling approach. These results are particularly counter intuitive given that value is traditionally considered proportional to risk. The reasons for these advantages can be attributed to the input data that the optimizer receives. By informing a solver with a smooth, estimated orebody model, it becomes far more difficult to discern ore from waste and can render the task of targeting well-connected, high grade zones far more difficult. Conditional spatial simulation not only better reproduces the statistical properties of the conditioning data, but allows for also allows for the quantification of risk, both of which a stochastic solver is able to exploit in full.

6 Conclusion

This work presents an approach to assess the geological uncertainty of REE deposits and integrate these uncertainties into the optimization of the mine production schedule. This approach is applied at a fictitious REE operation and the results show significant improvement both in terms of maximizing the value of the asset as well as mitigating the risk of deviating from annual production targets. SNESIM is used to quantify the volumetric uncertainty of the mineralized domain and MAF, integrated with DBSim, allows for the efficient joint conditional simulation of all the REE grades considered. The latter can provide an engineering team with the means to: assess the in-situ REE grade variability, reproduce the strong cross-element spatial relationships, and avoid the convention of using the TREO grade representation.

The SIP formulation is solved using an efficient implementation of the multi-neighbourhood tabu search metaheuristic in an amount of time that would be considered feasible in industry. The optimized stochastic mine production schedule is bench-marked against the industry's best known practices and is shown to increase the forecasted LOM NPV by 20%. The stochastic solution derives a schedule that yields a superior blend of REE bearing minerals at the head of the plant and a didymium product that is far more likely to meet the buyer's strict quality constraints. Future work would aim to test this approach on a real REE operation with more complex REE blending requirements.

References

Avalon Rare Metals Inc. (2013). Nechalacho Rare Earth Elements Project - Feasibility Study. NI 43-101 Technical Report, MICON International Ltd.

Birge, J. R., & Louveaux, F. (1997). Introduction to stochastic programming (2 Ed.): Springer.

Bley, A., Boland, N., Fricke, C., & Froyland, G. (2010). A strengthened formulation and cutting planes for the open pit mine production scheduling problem. Computers & Operations Research, 37, 1641–1647.

Boucher, A. (2009). Considering complex training images with search tree partitioning. Computers & Geosciences, 35(6), 1151–1158.

Boucher, A., & Dimitrakopoulos, R. (2009). Block Simulation of Multiple Correlated Variables. Mathematical Geosciences, 41(2), 215–237.

Caccetta, L., & Hill, S. P. (2003). An application of branch and cut to open pit mine scheduling. Journal of Global Optimization, 27(2-3), 349–365.

Commerce Resources Corp. (2012). Ashram Project - Preliminary Economic Assessment. NI 43-101 Technical Report, SGS Canada Inc.

David, M. (1988). Handbook of applied advanced geostatistical ore reserve estimation. Amsterdam; New York: Elsevier: Distributors for the United States and Canada Elsevier Science Pub. Co.

Desbarats, A. J., & Dimitrakopoulos, R. (2000). Geostatistical Simulation of Regionalized Pore-Size Distributions Using Min/Max Autocorrelation Factors. Mathematical Geology, 32(8), 919–942.

Dimitrakopoulos, R., & Grieco, N. (2009). Stope design and geological uncertainty: Quantification of risk in conventional designs and a probabilistic alternative. Journal of Mining Science, 45(2), 152–163.

Dimitrakopoulos, R., & Luo, X. (2004). Generalized sequential Gaussian simulation on group size ν and screen-effect approximations for large field simulations. Mathematical Geology, 36(5), 567–591.

Dimitrakopoulos, R., Martinez, L., & Ramazan, S. (2007). A maximum upside / minimum downside approach to the traditional optimization of open pit mine design. Journal of Mining Science, 43(1), 73–82.

Dimitrakopoulos, R., & Ramazan, S. (2004). Uncertainty-based production scheduling in open pit mining. SME Transactions, 316, 106–112.

Dimitrakopoulos, R., & Ramazan, S. (2008). Stochastic integer programming for optimising long term production schedules of open pit mines: methods, application and value of stochastic solutions. Mining Technology, 117(4), 155–160.

Ernst, & Young. (2010). Material risk - Access to technology minerals.

Gershon, M. E. (1983). Optimal mine production scheduling: evaluation of large scale mathematical programming approaches. International Journal of Mining Engineering, 1(4), 315–329.

Glover, F., & Laguna, M. (1997). Tabu Search: Kluwer Academic Publishers.

Godoy, M. (2003). The effective management of geological risk in long-term production scheduling of open pit mines. (Ph.D. Dissertation), University of Queensland, Brisbane, Australia.

Godoy, M., & Dimitrakopoulos, R. (2004). Managing risk and waste mining in long-term production scheduling of open-pit mines. SME Transactions, 316, 43–50.

Goodfellow, R., Albor Consuegra, F., Dimitrakopoulos, R., & Lloyd, T. (2012). Quantifying multi-element and volumetric uncertainty, Coleman McCreedy deposit, Ontario, Canada. Computers & Geosciences, 42, 71–78.

Goodfellow, R., & Dimitrakopoulos, R. (2014). Global optimization of open pit mining complexes with uncertainty. COSMO - Stochastic Mine Planning Laboratory. McGill University.

Goovaerts, P. (1993). Spatial orthogonality of the principal components computed from coregionalized variables. Mathematical Geology, 25(3), 281–302.

Goovaerts, P. (1997). Geostatistics for natural resources evaluation. New York: Oxford University Press.

Great Western Minerals Group Ltd. (2014). Steenkampskraal Rare Earth Element Project - Feasibility Study. NI 43-101 - Technical Report, Venmyn Deloitte.

Guardiano, F. B., & Srivastava, R. M. (1993). Multivariate Geostatistics: Beyond Bivariate Moments. In A. Soares (Ed.), Geostatistics Tróia '92: Springer Netherlands, 5, 133–144.

IAMGOLD. (2012). Niobec Mine Property - Preliminary Economic Assessment NI 43-101 - Technical Report, IAMGOLD Corporation.

Isaaks, E. H., & Srivastava, R. M. (1989). Applied Geostatistics. New York: Oxford University Press.

Journel, A. G. (1979). Geostatistical simulation - Ch. 6 Methods for exploration and mine planning. Engineering and Mining Journal, 180(12), 6.

Journel, A. G. (2007). Roadblocks to the evaluation of ore reserves - the simulation overpass and putting more geology into numerical models of deposits. Parkville Victoria: Australasian Inst Mining and Metallurgy.

Lamghari, A., & Dimitrakopoulos, R. (2012). A diversified Tabu search approach for the open-pit mine production scheduling problem with metal uncertainty. European Journal of Operational Research, 222(3), 642–652.

Lamghari, A., Dimitrakopoulos, R., & Ferland, J. A. (2014). A variable neighbourhood descent algorithm for the open-pit mine production scheduling problem with metal uncertainty. Journal of the Operational Research Society, 65(9), 1305–1314.

Matamc Explorations Inc. (2013). Kipawa Project - Feasibility Study. NI 43-101 - Technical Report, Roche Ltd.

Menabde, M., Froyland, G., Stone, P., & Yeates, G. (2007). Mining Schedule Optimisation for Conditionally Simulated Orebodies. AusIMM Spectrum Series, 14, 379–384.

Montiel, L. P., & Dimitrakopoulos, R. (2014). On globally optimizing a mining complex under supply uncertainty: integrating components from deposits to transportation systems. Ph.D. Thesis. McGill University, Montreal, Canada.

Molycorp Inc. (2012). Mountain Pass Rare Earth Project - Feasibility Study. NI 43-101 - Technical Report, SRK Consulting.

Quest Rare Minerals Ltd. (2014). Strange Lake Property - Preliminary Economic Assessment. NI 43–101 Technical Report, MICON International Ltd.

Ramazan, S., & Dimitrakopoulos, R. (2004). Recent applications of operations research and efficient MIP formulations in open pit mining. SME Transactions, 315, 73–78.

Ramazan, S., & Dimitrakopoulos, R. (2013). Production scheduling with uncertain supply: a new solution to the open pit mining problem. Optimization and Engineering, 14(2), 361–380.

Rondon, O. (2012). Teaching Aid: Minimum/Maximum Autocorrelation Factors for Joint Simulation of Attributes. Mathematical Geosciences, 44(4), 469–504.

Roskill. (2014). What does the WTO ruling mean for the Chinese rare earth industry? Roskill briefing paper.

Senécal, R., & Dimitrakopoulos, R. (2014). Long-term mine production scheduling with multiple processing destinations: a new and efficient multi-neighborhood tabu search metaheuristic implementation. COSMO - Stochastic Mine Planning Laboratory. McGill University.

Strebelle, S. (2002). Conditional Simulation of Complex Geological Structures Using Multiple-Point Statistics. Mathematical Geology, 34(1), 1–21.

Switzer, P., & Green, A. A. (1984). Min/max autocorrelation factors for multivariate spatial imagery. Standford University, Department of Statistics (6).

Vallée, M. (2000). Mineral resource + engineering, economic and legal feasibility = ore reserve. CIM Bulletin, 93(1038), 53–61.

Wackernagel, H. (2003). Multivariate geostatistics an introduction with applications (3 ed.). Berlin: Springer.